HHS Public Access

Author manuscript

Lab Chip. Author manuscript; available in PMC 2018 January 17.

Published in final edited form as:

Lab Chip. 2017 January 17; 17(2): 241–247. doi:10.1039/c6lc01430e.

3D printed metal molds for hot embossing plastic microfluidic devices

Tung-Yi Lin, **Truong Do**, **Patrick Kwon**, and **Peter B. Lillehoj***

Department of Mechanical Engineering, Michigan State University, East Lansing, MI, USA

Abstract

Plastics are one of the most commonly used materials for fabricating microfluidic devices. While various methods exist for fabricating plastic microdevices, hot embossing offers several unique advantages including high throughput, excellent compatibility with most thermoplastics and low start-up costs. However, hot embossing requires metal or silicon molds that are fabricated using CNC milling or microfabrication techniques which are time consuming, expensive and required skilled technicians. Here, we demonstrate for the first time the fabrication of plastic microchannels using 3D printed metal molds. Through optimization of the powder composition and processing parameters, we were able to generate stainless steel molds with superior material properties (density and surface finish) than previously reported 3D printed metal parts. Molds were used to fabricate poly(methyl methacrylate) (PMMA) replicas which exhibited good feature integrity and replication quality. Microchannels fabricated using these replicas exhibited leak-free operation and comparable flow performance as those fabricated from CNC milled molds. The speed and simplicity of this approach can greatly facilitate the development (i.e. prototyping) and manufacture of plastic microfluidic devices for research and commercial applications.

Graphical Abstract

We demonstrate a unique approach for fabricating plastic microfluidic devices via hot embossing using 3D printed metal molds.

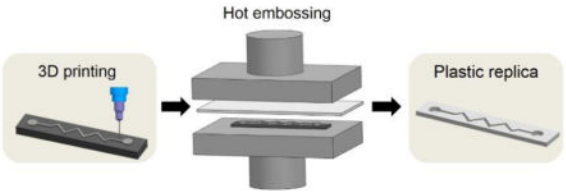

Introduction

Of all the materials available for fabricating microfluidic devices, plastics are one of the most favorable due to their low cost, excellent biocompatibility, high optical transparency

lillehoj@egr.msu.edu; Tel: +1-517-432-2976.

Electronic Supplementary Information (ESI) available: [details of any supplementary information available should be included here]. See DOI: 10.1039/x0xx00000x

and amenability to mass production [1]. Plastics are also compatible with many of the same surface functionalization treatments as polydimethylsiloxane (PDMS) and glass, enhancing their versatility for biological and analytical applications [2]. For these reasons, plastic microfluidic devices have been used for several important applications include *in vitro* diagnostics [3, 4], DNA analysis [5], tissue engineering [6] and drug discovery [7]. Currently, various methods exist for fabricating plastic microdevices with each offering its own unique set of advantages and disadvantages [8]. Injection molding, one of the earliest and most common methods, requires expensive machinery and custom dies for each application, making it poorly suited for low volume production. Recent efforts have focused on alternative fabrication techniques, including micromilling [9, 10], laser micromachining [11, 12], stereolithography [13] and 3D printing [14], which require lower startup costs and can be used for low volume production. While each of these methods are promising, they are limited to certain types of materials or result in diminished material properties (e.g. surface finish, optical transparency).

An alternative method that does not suffer from these limitations is hot embossing [15–18]. Hot embossing is a process where a pattern is mechanically stamped into a softened plastic substrate using a rigid mold. For microfluidics applications, molds are typically fabricated from metal or silicon using CNC milling or microfabrication techniques, such as photolithography [19], electroplating [20] and deep reactive ion etching (DRIE) [21]. However, these methods are time consuming, expensive and require skilled technicians. Other than metal and silicon, alternative mold materials have been demonstrated on embossed templates, such as PDMS [22, 23] and epoxy [24–26]. While these molds can be simpler to fabricate, they tend to suffer from poor reproducibility for multiple embossing cycles.

To address these limitations, we demonstrate for the first time the use of a 3D printed metal mold for hot embossing plastic microfluidic devices. Metal 3D printing is a recent innovation which offers many of the same advantages (e.g. simplicity, rapid production, high customization) as polymer 3D printing. However, one of the current limitations of metal 3D printing is that printed parts exhibit relatively low density (78%), large surface roughness (~50 μm) and intense residual stresses [27, 28], which greatly limits their utility for hot embossing microdevices. In this work, we use an improved Binder Jetting process (BJP) with optimized powder composition and processing parameters to generate 3D printed metal molds with no residual stress and significantly improved density and surface finish. The printed stainless steel molds were used to fabricate poly(methyl methacrylate) (PMMA) microchannels, which exhibited leak-free operation and comparable flow performance as microchannels fabricated from CNC milled molds. This unique approach offers a simpler and faster method for fabricating metal molds for hot embossing plastic microdevices suitable for both high and low volume (i.e. prototyping) manufacturing.

Experimental

Mold fabrication

Molds were designed using Siemens NX computer-aided design (CAD) software and printed using an X1-Lab 3D printer (ExOne, North Huntingdon, PA). This system uses a Binder

Jetting process (BJP) where a liquid polymer binder is selectively deposited on metallic powder in a layer-by-layer fashion using a roller. In contrast to other metal 3D printing techniques based on laser or electron beam sintering/melting, BJP allows decoupling of the printing and consolidation processes. Printing takes place at room temperature while the consolidation of parts can take place uniformly in a high temperature furnace. Thus, BJP does not induce residual stress or distortions in the part [29]. A modified processing protocol was used to improve the part density and surface finish as previously reported [30, 31]. Molds were fabricated using either a pure stainless steel (SS) 420 powder mixture, with average diameters of 30 μm (Oerlikon, Troy, MI) and 6 μm (Epson Atmix Corp., Hachinohe, Japan), or SS powder mixtures containing varying concentrations of 1 μm-diameter boron nitride (BN) powder (Sigma-Aldrich, St. Louis, MO). After printing, the molds were cured in an oven at 195°C. Loose powder was removed from the molds followed by sintering in an argon-filled furnace at 1250°C (Materials Research Furnaces Inc., Suncook, New Hampshire).

Surface roughness and replication fidelity measurements

Surface roughness and replication fidelity measurements of printed molds and embossed replicas were carried out using an Olympus FluoView FV1000 confocal laser scanning microscope (CLSM). CLSM scans were collected using a 20× objective (NA = 0.75) scanning at 0.2 μm increments through 120 μm sample thicknesses at a resolution of 256 × 256 pixels. Surface profile images were generated from stacked CLSM scans and processed using MATLAB as previously described [32]. Surface roughness measurements were calculated from surface profile images based on the technique described in [33].

Hot embossing

Plastic replicas were generated using 1.5 mm-thick PMMA sheets purchased from McMaster-Carr (Elmhurst, IL). Prior to molding, PMMA was rinsed with 2-propanol, deionized (DI) water and dried with N_2 gas. Hot embossing was performed at 1 ton and 120°C for 30 min using a Carver hot press (Wabash, IN). The temperature was lowered to 90°C for demolding. The demolding temperature was carefully controlled to ensure adequate surface completion and replication quality [34]. Plate alignment was checked before embossing to ensure uniform force distribution on the PMMA part and the embossing temperatures were closely monitored throughout the process via a thermocouple.

Microchannel fabrication

To generate enclosed microchannels, PMMA replicas were thermally bonded to 1.5 mm-thick PMMA pieces using a Carver hot press. Through-holes were generated using a CO_2 laser cutter (Universal Laser Systems, Scottsdale, AZ) to create inlets and outlets. Prior to bonding, PMMA surfaces were treated with UV/O_3 for 40 min using a Novascan Technologies UV/O_3 cleaner (Ames, IA). In addition to making the surfaces more hydrophilic, UV/O_3 treatment enables bonding to occur at lower temperatures which minimizes the likelihood of channel collapsing or deformation [35, 36]. PMMA pieces were sandwiched between Al foil to ensure uniform heat distribution and facilitate alignment in the press. The plates were preheated to 80°C, followed by the application of 1 ton for 10 min. Afterwards, the plates were cooled to room temperature and the bonded devices were

released. Bonding temperatures were closely monitored throughout the process via a thermocouple.

Microchannel characterization

PMMA microchannels were cut normal to their length using a dicing saw (Buehler, Illinois) and cross-sectional images were captured using a JEOL 6620LV scanning electron microscope (SEM) at 10 kV with 50× magnification. For flow comparison studies, PMMA microchannels were also fabricated from stainless steel molds manufactured by CNC milling. The parameters for hot embossing and thermal bonding were kept consistent for both the 3D printed and CNC milled molds. Color dyes were dispensed into the inlets of the microchannels using a pipette and fluid flows were captured using a video camera, which were analyzed for flow rate measurements. Studies to compare pressure-driven flows in 3D printed and CNC milled molds were carried out by infusing PMMA microchannels with a solution of 10-μm diameter polystyrene beads (Sigma, St. Louis, MO) in phosphate buffer solution (PBS) at a concentration of 10^5 particles/mL. Solutions were infused at a constant rate of 10 μL/min using a KD Scientific syringe pump (Holliston, MA). Flow rates were calculated by tracking the average bead velocity from video recordings.

Results and discussion

Fabrication and characterization of 3D printed molds

A major limitation of current metal 3D printing technologies, including BJP, is the relatively poor surface finish of printed parts. For hot embossing, a smooth mold surface is required to facilitate the release of the plastic replica without damaging the embossed features. The surface finish of 3D printed parts can be improved by using very fine powders since thinner deposition layers can be achieved [37, 38]. However, many 3D printing technologies, including BJP, are constraint to a certain particle size range as the roller is unable to spread uniform powder layers. To address these issues, we used a mixture of SS powder with two distinct powder sizes which allows the smaller particles to become nested in the interstitial spacing of the larger particles, as previously reported [39]. Through a series of experimental trials, a powder mixture of 60% of 30 μm particles and 40% of 6 μm particles yielded the optimal surface finish and density. While the incorporation of smaller particles in the powder mixture greatly improves the surface finish, having too much fine powder can hinder the printing process. Therefore, further enhancements in the surface finish were obtained by adding minute concentrations of BN powder which reduces the consolidation temperature and locally promotes liquid formation during sintering.

Despite its major advantage in minimizing residual stress, BJP suffers from relatively low part density due to incomplete densification of the powder, even at elevated temperatures. To enhance the mechanical strength of the mold and embossing reproducibility, molds should be near full density. The maximum achievable density we obtained using pure SS powder was 78%, even when sintered at 1400°C for 6 hr. The final part density was significantly improved by incorporating BN powder. Based on prior experimental studies [31], adding 0.5% wt. BN to the SS powder mixture increased the final part density to 93% at a lower sintering temperature of 1250°C with negligible distortion.

Photographs and CLSM surface profiles of 3D printed molds with varying concentrations of BN are shown in Fig. 1. The colors in the surface profile images represent the surface roughness (measured in the z-dimension). While the mold and replica generated from the pure SS powder appears smoother in the photographs than those generated from powder containing BN, this is an aberration due to differences in the contrast between the SS and BN powder which results in a specked surface pattern. The differences in surface morphology between the molds can be clearly seen in the corresponding surface profile images. The pure stainless steel mold (Fig. 1a) exhibited an average surface roughness, R_a, of 6.61 μm ± 0.71 μm. In contrast, molds containing 0.25%, 0.5% and 0.75% wt. BN exhibited improved surface finishes with R_a values of 3.83 μm ± 0.53 μm, 3.65 μm ± 0.48 μm and 3.86 μm ± 0.86 μm, respectively (Figs. 1b–d). These values are 2× lower than the pure SS mold and up to 13× lower than previously reported 3D printed metal parts [27], and demonstrates that the addition of BN greatly improves the surface finish. However, a higher concentration of BN powder did not seem to have a significance impact on further improving the surface roughness. To further validate these results, we also performed surface characterization of the molds using a contact profilometer. As shown in Fig. S1, the mold containing 0.25% BN exhibits a substantially smoother surface than the pure SS mold, which is consistent with our surface profile images and R_a measurements.

We also compared the transfer accuracy between the CAD design and the printed molds, as shown in Table S1 in Supplementary Information. The transfer accuracy in the lateral dimension (i.e. feature width) for all the molds was similar (80.6%–85%), which is due to the burn off of the binder and densification. In contrast, molds containing higher concentrations of BN resulted in a substantially diminished transfer accuracy in the vertical dimension (i.e. feature height). For example, the channel height of the mold containing 0.25% wt. BN was reduced by 12.6% compared to the CAD design whereas it was reduced by 82.5% for the mold containing 0.75% wt. BN. Since the additional BN reduces the overall melting temperature and promotes local liquid formation, we hypothesize that higher concentrations of BN causes the features to collapse during sintering. Based on these results, SS with 0.25% wt. BN was selected as the optimal mold material. While the pure SS mold offers a slightly higher transfer accuracy, the improvements in surface finish and mold density offered by the mold containing 0.25% wt. BN are more important for generating high quality replicas for microfluidic devices. To accommodate for the slight loss in transfer accuracy, the mold can simply be designed with compensated dimensions. To validate this concept, we designed a 400 μm × 500 μm (W × H) microchannel with compensated dimensions of 330 μm and 570 μm (W × H) and printed five copies using SS with 0.25% wt. BN. The actual dimensions of the printed molds were 395.8 ± 8.33 μm × 501.2 μm ± 14.4 μm (W × H) (Fig. S4 in Supplementary Information), resulting in average transfer accuracies of 98.9% and 99.8% for the width and height, respectively. These results are presented in Table S2 and demonstrate that microchannels with accurate dimensions can be fabricated using 3D printed molds by compensating for the difference in the design.

Characterization of PMMA replicas

A typical hot embossing process involves four main steps: (1) heating the mold and substrate to the molding temperature (above the glass transition temperature, T_g of the substrate), (2)

applying pressure to transfer the mold pattern to the substrate, (3) cooling the mold and substrate to the demolding temperature, and (4) demolding the replica. During this process, thermoplastics undergo two stages: the first is the deformation stage that occurs during embossing, and the second is the recovery stage that occurs during demolding. In this work, PMMA with a T_g of 103°C was used. The embossing temperature, force and duration are three important parameters that influence the quality of the replica. The embossing duration was fixed at 30 min since this time allows for good surface completion, as previously reported [40], while minimizing the overall processing time. The embossing temperature and force were briefly studied and the results are presented in Fig. S2. Embossing at 110°C and 0.5 tons resulted in poorly defined features and a visibly rough surface finish (Fig. S2a). However, increasing the embossing temperature and force to 120°C and 1 ton, respectively, resulted in sharper features and an overall smoother surface (Fig. S2b). These parameters were selected for subsequent embossing procedures for the remainder of this work. For the demolding stage, there are several issues commonly associated with embossing micro-sized features such as stiction and corresponding distortion/damage of the features [41]. These complications are mainly due to adhesion between the mold and substrate which is correlated with the demolding temperature [34]. A higher demolding temperature will result in faster demolding while a lower temperature will result in lower adhesion. A demolding temperature of 90°C was found to result in negligible adhesion while minimizing the processing time to < 1 hr.

To assess the functionality of 3D printed molds for hot embossing, we first studied the surface finish of the replicas. Photographs and CLSM surface profiles of PMMA replicas fabricated from 3D printed molds are shown in Fig. 2. The surface roughness of the replicas follow closely with those of the corresponding molds (Fig. 1). Replicas fabricated from the pure SS mold exhibited a R_a of 8.23 μm ± 0.53 μm (Fig. 2a) while replicas fabricated from molds containing 0.25%, 0.50% and 0.75% BN had substantially lower R_a values of 4.7 μm ± 0.84 μm, 4.20 μm ± 0.73 μm, and 4.12 μm ± 1.1 μm, respectively (Figs. 2b–d). In addition to improving the surface finish, the inclusion of BN also helped to minimize the presence of defects at the edges of the embossed features that are typically generated during demolding (Fig. 3). We also briefly studied the replication accuracy between the printed mold and replica after hot embossing (Table 1). Replicas generated from the pure stainless steel mold exhibited replication accuracies of ~83% in both the lateral and vertical dimensions. However, molds containing BN resulted in enhanced replication accuracy ranging from 91%–97% with no significant difference among molds with different concentrations of BN. These improvements are likely due to the enhanced surface finish of the printed mold, facilitating mold transfer and demolding.

Thermal bonding and the influence of surface roughness

To generate enclosed microchannels using embossed components, replicas were bonded to flat pieces of PMMA. There are various methods for bonding plastics including solvent bonding [42, 43], thermal bonding [44] and adhesive layer bonding [45]. Of these, thermal bonding is a simple approach which can generate a strong and permanent bond. However, thermal bonding requires high temperatures and forces which can deform or damage plastic features. To mitigate this issue, a UV/O_3 surface treatment was applied to the PMMA

surfaces prior to bonding. UV/O_3 breaks down the polymer chains and produces more oxygen-containing functional groups on plastic surfaces which improves the overall bonding strength [46]. Therefore, lower bonding temperatures can be used which helps to preserve the embossed features.

The surface roughness of the embossed part plays an important role in the bonding process. Therefore, we evaluated the bond quality of PMMA microchannels generated using replicas fabricated from 3D printed molds. The integrity of the embossed features after bonding was examined by observing the channel cross section using SEM (Fig. 4). Replicas generated using the pure stainless steel mold at 80°C resulted in incomplete bonding, as evident by the interfacial gap as shown in Fig. 4a. Fully enclosed microchannels could be generated at higher bonding temperatures (90°C), however, there is evidence of substantial microchannel deformation and shrinking (Figs. 4b). However, leak-free bonding could be achieved at 80°C using the mold containing 0.25% wt. BN with minimal channel deformation (Fig. 4c). These results are consistent with previous reports on the integrity of thermally bonded thermoplastic microfluidic devices treated with UV/O_3 [47]. The difference in the surface roughness of the embossed parts is quite apparent in regards to bonding microfluidic devices where replicas fabricated from the mold containing 0.25% wt. BN could be bonded at lower temperatures with improved microchannel integrity compared with those fabricated from the pure SS mold.

Mold reproducibility for multiple embossing cycles

Experiments were performed to evaluate the reproducibility of 3D printed molds for multiple embossing cycles. A single mold was used to fabricate PMMA replicas for up to 40 embossing cycles and optical images of the microchannel features were taken at regular intervals to monitor the mold integrity and replication quality. Measurements of the channel dimensions were also performed to quantify any changes resulting from multiple embossing cycles. The results are presented in Fig. S3 in Supplementary Information. As shown in Fig. S3a & b, the mold and replicas maintain sharp features with no signs of defects of deformations even after 40 embossing cycles. Furthermore, the channel dimensions remain consistent throughout the duration of the study (Fig. S3c). While we stopped this study at 40 cycles due to time constraints, these results suggest that 3D printed molds can maintain their integrity for many additional embossing cycles with negligible loss in replication quality. In contrast, PDMS molds have limited lifetime of ~20 cycles [48].

Microchannel testing

To evaluate the functionality of microfluidic devices embossed using 3D printed metal molds, PMMA microchannels were fabricated and tested using colored dyes. Due to the UV/O_3 treatment prior to thermal bonding, the inner surfaces of the microchannels were made hydrophilic and liquids could be driven inside the channels via capillary flow. We tested two different shaped microchannels: serpentine and zig-zag. As shown in Fig. 5a, colored dyes quickly filled both microchannels with no observable leaking. To further validate the capabilities of microdevices fabricated from 3D printed molds, straight microchannels were tested with pressure-driven flows and visually monitored over time. As

shown in Fig. 5b, there are no signs of leaking after 1, 5, 10 and 20 mins of continuous fluid flow and provides further evidence that these devices exhibit leak-free operation.

Experiments were also performed to compare the flow performance in straight microchannels fabricated from molds generated using 3D printing and CNC milling, as a benchmark. We first measured the capillary flow rate in three different channel widths (200 μm, 400 μm and 800 μm) using DI water. As shown in Fig. 6, capillary flow rates for microchannels fabricated from 3D printed molds were comparable to those fabricated from the CNC milled mold. We also used PMMA microchannels for pressure-driven flows and measured the average flow velocities. These results are consistent with the capillary flow rate measurements and shows that there is no significant difference between flow rates in microchannels fabricated from 3D printed molds and CNC milled molds. A few of the data points exhibit larger standard deviations which we attribute to experimental errors in estimating the flow rates. Nonetheless, these results indicate that plastic microfluidic devices fabricated from 3D printed molds offer nearly identical flow performance as those fabricated from traditional manufacturing methods (i.e. CNC milling).

Conclusions

We have demonstrated a unique approach for fabricating plastic microfluidic devices via hot embossing using 3D printed metal molds. Metal 3D printing is a promising and rapidly growing technology which offers several advantages over existing fabrication techniques for generating hot embossing molds. Using optimized powder composition and processing parameters, we were able to generate 3D printed molds with superior material properties and replication accuracy. Specifically, we show that a stainless steel powder mixture incorporating 0.25% wt. BN powder dramatically improves the part density and surface finish. These enhancements enable for smoother surface finish of the plastic replicas and improved integrity of the embossed features. PMMA microchannels fabricated using this method exhibited leak-free operation with comparable flow performance as microchannels fabricated from CNC milled molds for both capillary and pressure-driven flows. In summary, this unique approach offers a rapid and simplified method for generating metal molds for embossing plastic microfluidic devices which can be used for high and low volume (i.e. prototyping) production in research and commercial applications.

Supplementary Material

Refer to Web version on PubMed Central for supplementary material.

Acknowledgments

This work was support by the National Institutes of Health (R01AI113257). We thank Dinh S. Nguyen for his assistance with surface roughness measurements.

Notes and references

1. Chin CD, Linder V, Sia SK. Lab Chip. 2012; 12:2118. [PubMed: 22344520]
2. Illa X, Ordeig O, Snakenborg D, Romano-Rodriguez A, Compton RG, Kutter JP. Lab Chip. 2010; 10:1254–1261. [PubMed: 20445877]

3. Ko JS, Yoon HC, Yang H, Pyo HB, Chung KH, Kim SJ, Kim YT. Lab Chip. 2003; 3:106–113. [PubMed: 15100791]
4. Kim DS, Lee SH, Ahn CH, Lee JY, Kwon TH. Lab Chip. 2006; 6:794–802. [PubMed: 16738733]
5. Wu J, Chantiwas R, Amirsadeghi A, Soper AA, Park S. Lab Chip. 2011; 11:2984–2989. [PubMed: 21779601]
6. Tao S, Young C, Redenti S, Zhang Y, Klassen H, Desai T, Young MJ. Lab Chip. 2007; 7:695–701. [PubMed: 17538710]
7. Lin Y-S, Huang K-S, Yang C-H, Wang C-Y, Yang Y-S, Hsu H-C, Liao Y-J, Tsai C-W. Plos One. Mar.2012 7
8. Becker H, Locascio LE. Talanta. 2002; 56:267–287. [PubMed: 18968500]
9. Guckenberger DJ, de Groot TE, Wan AMD, Beebe DJ, Young EWK. Lab Chip. 2015; 15:2364–2378. [PubMed: 25906246]
10. Wilson ME, Kota N, Kim YT, Wang Y, Stolz DB, LeDuc PR, Ozdoganlar OB. Lab Chip. 2011; 11:1550–1555. [PubMed: 21399830]
11. Wang SC, Lee CY, Chen HP. J Chromatogr A. 2006; 1111:252–257. [PubMed: 16288768]
12. Klank H, Kutter JP, Geschke O. Lab Chip. 2002; 2:242–246. [PubMed: 15100818]
13. Au AK, Lee W, Folch A. Lab Chip. 2014; 14:1294–1301. [PubMed: 24510161]
14. Kitson P, Rosnes M, Sans V, Dragone V, Cronin L. Lab Chip. 2012; 12:3267–3271. [PubMed: 22875258]
15. Zhao Y, Cui T. J Micromech Microeng. 2013; 13:430–435.
16. Esch MB, Kapur S, Irizarry G, Genova V. Lab Chip. 2003; 3:121–127. [PubMed: 15100793]
17. Miserere S, Mottet G, Taniga V, Descroix S, Viovy JL, Malaquin L. Lab Chip. 2012; 12:1849–1856. [PubMed: 22487893]
18. Kricka LJ, Fortina P, Panaro NJ, Wilding P, Alonso-Amigo G, Becker H. Lab chip. 2002; 2:1–4. [PubMed: 15100847]
19. Greener J, Li W, Ren J, Voicu D, Pakharenko V, Tang T, Kumacheva E. Lab Chip. 2010; 10:522–524. [PubMed: 20126695]
20. Novak R, Ranu N, Mathies RA. Lab Chip. 2013; 13:1468–1471. [PubMed: 23450308]
21. Xia Q, chou SY. Nanotechnology. 2008; 19:455301. [PubMed: 21832766]
22. Goral VN, Hsieh YC, Petzold ON, Faris RA, Yuen PK. J Micromech Microeng. 2011; 21:017002.
23. Fiorini GS, Jeffries GDM, Lim DSW, Kuyper CL, Chiu DT. Lab chip. 2003; 3:158–163. [PubMed: 15100767]
24. Koerner T, Brown L, Xie R, Oleschuk RD. Sens Actuators, B. 2005; 107:632–639.
25. Jena RK, Yue CY, Yun KX. RSC Adv. 2014; 4:12448–12456.
26. Young EWK, Berthier E, Guckenberger DJ, Sackmann E, Lamers C, Meyvantsson I, Huttenlochers A, Beebe DJ. Anal Chem. 2011; 83(4):1408–1417. [PubMed: 21261280]
27. Sandron S, Heery B. Analyst. 2014; 139:6343–6347. [PubMed: 25285334]
28. Gibson I, Rosen DW, Stucker B. Springer. 2010:216.
29. Mostafaei A, Stevens EL, Hughes ET, Biery SD, Hilla C, Chmielus M. Mater Des. 2016; 108:126–135.
30. Sun L, Kim YH, Kim D, Kwon P. J Manuf Sci Eng. 2009; 131:6.
31. Do T, Shin C, Stetsko D, VanConant G, Vartanian A, Pei S, Kwon P. Procedia Manufacturing. 2015; 1:263–272.
32. Olortegui-Yume JA, Kwon PY. Wear. 2010; 268:493–504.
33. Young PL, Brackbill TP, Kandlikar SG. Proc of the 5th ICNMM2007. :827–836.
34. Dirckx ME, Hardt DE. J Micromech Microeng. 2011; 21:085024.
35. Tsao CW, Hromada L, Liu J, Kumar P, DeVoe DL. Lab Chip. 2007; 7:499–505. [PubMed: 17389967]
36. Bhattacharyya A, Klapperich CM. Lab chip. 2007; 7:876–882. [PubMed: 17594007]
37. Vaezi M, Chua CK. Int J Adv Manuf Technol. 2011; 53:275–284.
38. Lu K, Hiser M, Wu W. Powder Technol. 2009; 192:178–183.

39. Lanzetta M, Sachs E. Rapid Prototyping Journal. 2003; 9(3):157–166.
40. Becker H, Heim U. Sensors and Actuators A. 2000; 83:130–135.
41. Cameron NS, Roberge H, Veras T, Jakeway SC, Crabtree HJ. Lab chip. 2006; 6:936–941. [PubMed: 16804599]
42. Kricka LJ, Fortinab P, Panaroa NJ, Wildinga P, Alonso-Amigoc G, Becker H. Lab Chip. 2002; 2:1–4. [PubMed: 15100847]
43. Brown L, Koerner T, Horton JH, Oleschuk RD. Lab Chip. 2006; 6:66–73. [PubMed: 16372071]
44. Sun Y, Kwok YC, Nguyen NT. J Micromech Microeng. 2006; 16:1681–1688.
45. Hamad EM, Bilatto SER, Adly NY, Correa DS, Wolfrum B, Schoning MJ, Offenhausser A, Yakushenko A. Lab Chip. 2016; 16:70–74. [PubMed: 26627046]
46. Peeling J, Clark DT. J Polym Sci, Chem Ed. 1983; 21:2047.
47. Tsao CW, De Voe DL. Microfluid Nanofluid. 2009; 6:1–16.
48. Narasimhan J, Papautsky I. J Micromech Microeng. 2003; 14:96–103.

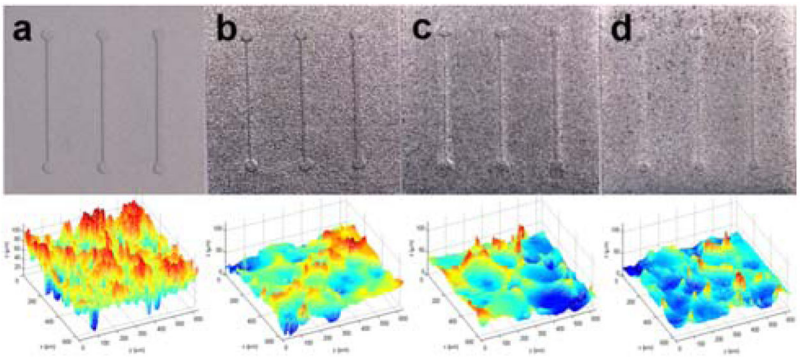

Figure 1.

Photographs (upper) and surface profiles (lower) of 3D printed molds containing 0% (a), 0.25% (b), 0.5% (c) and 0.75% (d) wt. BN. The scan size and z-scale are 600 μm × 600 μm and 120 μm, respectively.

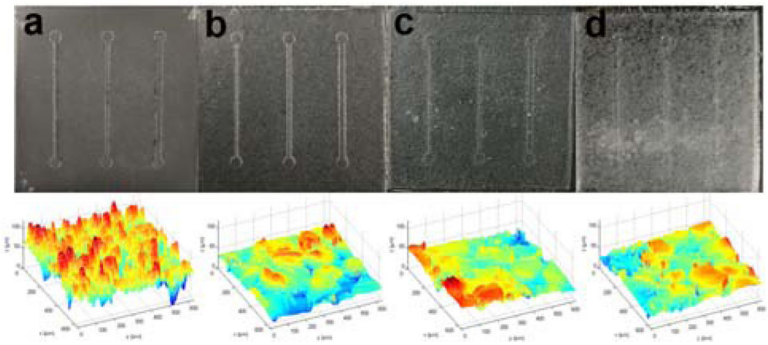

Figure 2.

Photographs (upper) and surface profiles (lower) of PMMA replicas fabricated from 3D printed molds containing 0% (a), 0.25% (b), 0.5% (c) and 0.75% (d) wt. BN. The scan size and z-scale are 600 μm × 600 μm and 120 μm, respectively.

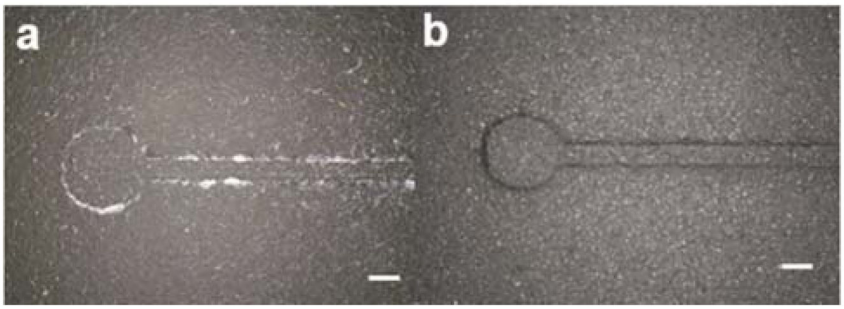

Figure 3.

Close up images of embossed microfluidic features in PMMA fabricated using the pure stainless steel mold (a) and mold containing 0.25% wt. BN (b). Hot embossing was performed at 120°C and 1 ton for 30 min. Scale bars, 500 μm

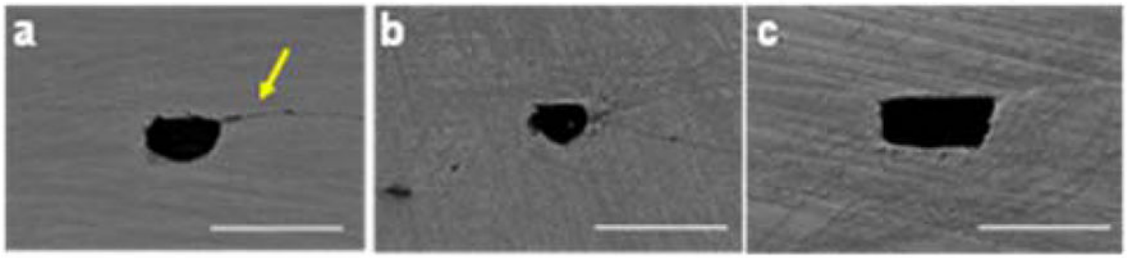

Figure 4.

SEM images of cross sections of PMMA microchannels fabricated using the pure stainless steel mold and thermally bonded at 80°C (a), 90°C (b) and the mold containing 0.25% wt. BN at 80°C (c). The arrow indicates incomplete bonding. Scale bars, 500 μm.

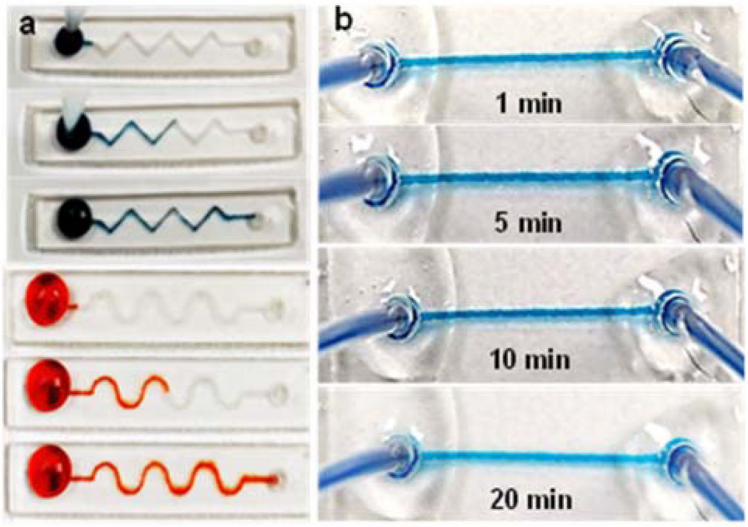

Figure 5.

(a) Capillary flow in PMMA microchannels fabricated from 3D printed molds. Colored dye is dispensed at the inlet of the chips using a pipette. (b) Pressure-driven flow inside a PMMA microchannel fabricated from a 3D printed mold. Colored dye is pumped into the microchannel using a syringe pump at rate of 50 μL/min. Photographs at 1, 5, 10 and 20 min during continuous flow.

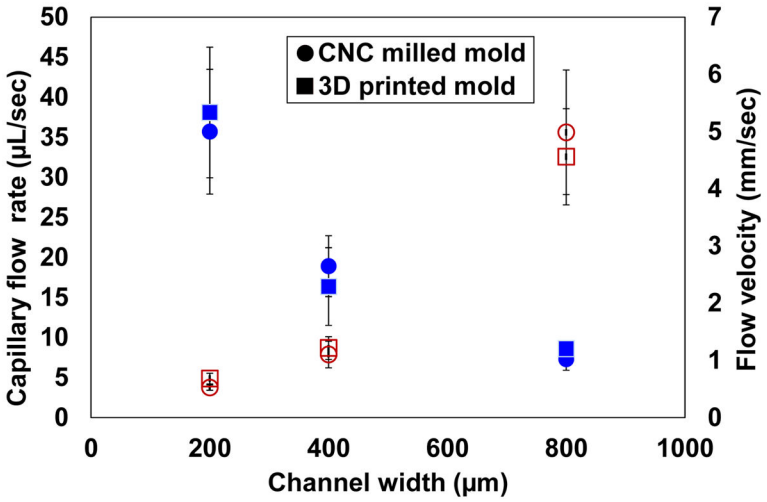

Figure 6.

Comparison of flow performance in PMMA microchannels fabricated from 3D printed molds (squares) and CNC milled molds (circles). Capillary flow rates and pressure-driven flow rates are plotted as hollow and solid markers, respectively. Each data point represent the mean ± SD of three measurements for capillary flow experiments and five measurements for pressure-driven flow experiments.

Table 1

Replication accuracy between the mold and replica after hot embossing

% wt. BN	Width	Height
0	82.7%	82.5%
0.25	90.6%	96.6%
0.50	92.8%	93.8%
0.75	91.3%	90.7%